

Thermomechanical fatigue – Damage mechanisms and mechanism-based life prediction methods

H-J CHRIST, A JUNG, H J MAIER and R TETERUK

Institut für Werkstofftechnik, Universität Siegen, D-57068 Siegen, Germany
e-mail: Christ@ifwt.mb.uni-siegen.de

Abstract. An existing extensive database on the isothermal and thermomechanical fatigue behaviour of high-temperature titanium alloy IMI 834 and dispersoid-strengthened aluminum alloy X8019 in SiC particle-reinforced as well as unreinforced conditions was used to evaluate both the adaptability of fracture mechanics approaches to TMF and the resulting predictive capabilities of determining material life by crack propagation consideration. Selection of the correct microstructural concepts was emphasised and these concepts were, then adjusted by using data from independent experiments in order to avoid any sort of fitting. It is shown that the cyclic J -integral (ΔJ_{eff} concept) is suitable to predict the cyclic lifetime for conditions where the total crack propagation rate is approximately identical to pure fatigue crack growth velocity. In the case that crack propagation is strongly affected by creep, the creep-fatigue damage parameter Δ_{CF} introduced by Riedel can be successfully applied. If environmental effects are very pronounced, the accelerating influence of corrosion on fatigue crack propagation can no longer implicitly be taken into account in the fatigue crack growth law. Instead, a linear combination of the crack growth rate contributions from plain fatigue (determined in vacuum) and from environmental attack is assumed and found to yield a satisfactory prediction, if the relevant corrosion process is taken into account.

Keywords. Thermomechanical fatigue; life prediction; fracture mechanics; fatigue crack propagation; IMI 834; X8019.

1. Introduction

Cyclic loading of metallic materials at high temperature is known to cause a complex evolution of damage which can hardly be described in a unique, simple and straightforward manner. This statement holds true even more correctly in the case that a component is subjected to thermomechanical fatigue (TMF) loading conditions which often result in service from a combination of thermal transients during startup and shutdown with mechanical strain cycles. Such complex cycling may lead to damage contributions from environmental degradation (usually termed *oxidation*), *fatigue*, and *creep*. The individual extent of these damage constituents and their mutual and synergistic interactions depend very strongly on the specific material considered and the loading conditions applied.

Driven by the need for an accurate concept to predict life expectancy of metallic materials subjected to complex loading conditions, as this is a prerequisite for improving reliability and economy of the use of such materials, a variety of life prediction models have already been proposed for TMF (e.g. Woodford & Mowbray 1974; Halford & Manson 1976; Skelton 1983; Okazaki & Koizumi 1983; Jordan & Meyers 1986; Danzer 1988; Chaboche & Lesne 1988; Neu & Sehitoglu 1989; Miller *et al* 1993; Rémy *et al* 1993; Bernstein *et al* 1993; ASME 1994; Ellison & Al-Zamily 1994; Dai *et al* 1996; Kadioglu & Sehitoglu 1996; Zamrik & Renauld 2000; Halford *et al* 2000). In order to take the complex interaction of fatigue, creep and oxidation into account, many different concepts have been used which can basically be subdivided into four classes, (i) empirical, (ii) damage mechanics, (iii) fracture mechanics and (iv) physical models (Danzer 1988). Currently, the significance of physical models for TMF life prediction is rather low. This can mainly be attributed to the problem of modelling the interaction of damage mechanisms, where still sound physical concepts are missing. The importance of the physical approach lies primarily in providing the physical background for empirical and damage mechanics models, e.g. by explaining the conditions which promote the formation of cavities. While the concept of damage mechanics is rarely applied to complex loading (e.g. Chaboche & Lesne 1988), phenomenological (empirical) approaches are often used (Woodford & Mowbray 1974; Halford & Mason 1976; Bernstein *et al* 1993; Ellison & Al-Zamily 1994; Zamrik & Renauld 2000; Halford *et al* 2000) and preferred in practical application for design purposes (ASME 1994). However, despite the fact that often a reasonable agreement between experimentally observed TMF life and the data predicted by means of empirical models is reported, the shortage of a physical basis seems to be not only unsatisfactory but also dangerous if the model parameters are transferred to deviating loading conditions.

Fracture mechanics concepts describe the growth of a fatal crack from its initial size to its final size at failure. These methods are preferentially applicable if a material contains flaws from the start or if cracks are initiated quickly at the beginning of cyclic life. The local conditions at or in the vicinity of the crack tip are considered to be responsible for crack propagation and hence parameters such as K , J and C^* and their cyclic counterparts are applied, since they can be determined on a macroscopic level. The striking advantage of fracture mechanics methods is that crack length represents a simple and physically reasonable quantity of damage. Furthermore, the implications of microstructural changes can directly be taken into account in modelling. Hence, from the point of view of transferability and predictive capability these models appear to be most versatile for complex loading situations such as TMF. This benefit seems to be important, as corresponding laboratory tests are usually run under more severe conditions than those encountered in service of an actual high-temperature component. Consequently, fracture mechanics has been applied to TMF loading in several studies (e.g. Skelton 1983; Okazaki & Koizumi 1983; Jordan & Meyers 1986; Miller *et al* 1993; Dai 1996; Kadioglu & Sehitoglu 1996).

The objective of the present paper is to provide a compact survey of the applications of life prediction methods based on fracture mechanics concepts to isothermal and thermomechanical fatigue conditions carried out in a series of studies performed in the laboratory of the authors (Pototzky 1999; Jung 2000; Teteruk 2001). Emphasis is made in two areas the first area being the selection and adaptation of models according to the relevant material-specific damage mechanisms as identified by means of thorough microstructural analysis. The second area is the expansion of these models with respect to TMF. For brevity, the paper is restricted to fracture mechanics concepts, while the results obtained by application of selected damage mechanics and empirical methods are reported elsewhere (Maier *et al* 2002).

2. Details on the materials and experimental procedures

2.1 Materials considered

The investigation was performed on three metallic materials which basically fulfill the requirement of a short crack initiation stage. The first alloy was high-temperature titanium alloy IMI 834 which is a near- α Ti alloy of nominal composition Ti-5.8Al-4.0Sn-3.5Zr-0.7Nb-0.5Mo-0.35Si-0.06C (in wt %). All data used in this study were obtained on the bimodal microstructure which is considered to yield an optimum compromise between creep and fatigue performance (Neal 1985). Figure 1 shows an optical micrograph of this microstructure which was established by solution annealing the material for 2 h at 1020°C, i.e., within the $\alpha + \beta$ phase field, in vacuum followed by a rapid oil quench. During quenching the β phase transforms into lamellar α (transformed β) embedding the primary α grains. The average grain size and the volume fraction of the primary α grains were found to be 14 μm and 15 vol. pct, respectively, whereas the transformed β grains show a grain size of about 25 μm . Prior to mechanical testing, the material was aged for 2 hours at 700°C and air cooled. This improves the mechanical properties due to the precipitation of fine silicide particles and ordered Ti_3Al .

The second and third alloy employed in this study were the high-temperature aluminum alloy X8019/12.5_p (nominal composition Al-8Fe-4Ce in wt pct) which is reinforced with 12.5 vol. pct SiC particles and the unreinforced (i.e., SiC-free) reference alloy. Both alloys are dispersion-strengthened and have an excellent microstructural stability at elevated temperature (Angers *et al* 1987). Dispersion strengthening is obtained by rapid solidification of the gas-atomized powder as part of the powder-metallurgy production route leading to

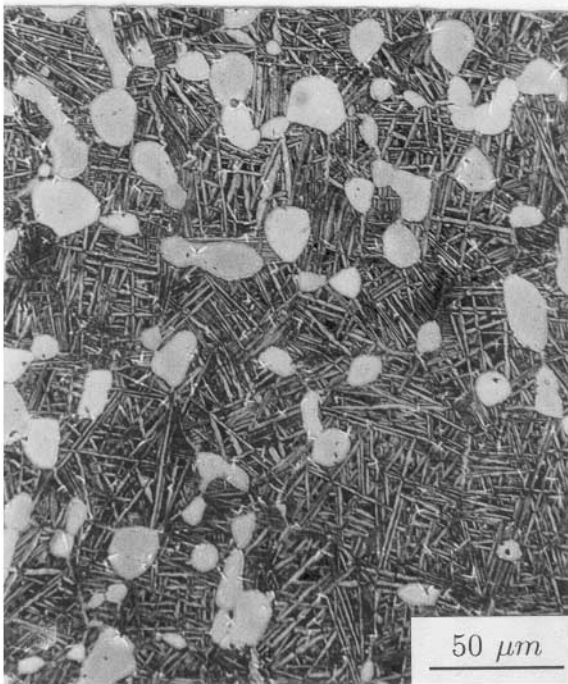


Figure 1. Optical micrograph of the bimodal microstructure of IMI 834.

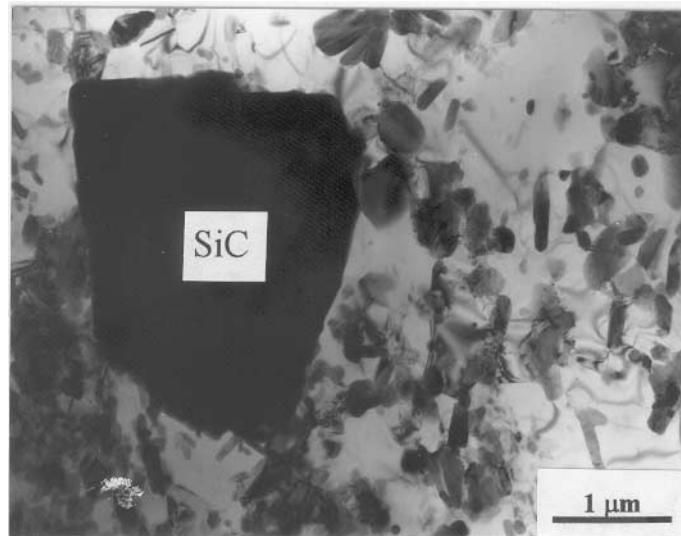


Figure 2. TEM micrograph of X8019/12.5_p showing an SiC particle and dispersoids.

a high volume fraction of fine intermetallic phases formed by iron, cerium and aluminum. Transmission electron microscopy (TEM) indicated that the microstructure of both alloys is identical regarding fraction and morphology of these dispersoids and also regarding grain size which was found to be about 1 μm. Figure 2 shows a TEM image of the particle-reinforced variant.

The SiC particles present in this material were found to have an average diameter of about 3 μm and appear to have no effect on the dispersoid distribution. Metallographic inspection revealed an excellent bonding at the SiC/matrix interface and a homogeneous distribution of both the dispersoids and the SiC reinforcement.

2.2 Experimental procedure

The fatigue tests were carried out in servohydraulic testing machines (MTS) equipped with induction heating systems on specimens with a cylindrical gauge length, which were either mechanically (X8019 and X8019/12.5_p) or electrochemically (IMI 834) polished prior to testing. All TMF experiments and the isothermal fatigue tests were performed under symmetrical push-pull closed-loop plastic strain control using a triangular function generator signal. This technique ensures that the specimens were always deformed at a constant (absolute value of) plastic strain rate facilitating the comparison of the behaviour under TMF and isothermal test conditions (Christ *et al* 1996). In the TMF experiments, the temperature was varied linearly with time and synchronously in-phase (IP) and out-of-phase (OP) to the plastic strain. The tests were always started at the mean temperature and at zero plastic strain with the strain increasing. The majority of the fatigue tests were conducted in laboratory air; though some experiments were carried out in high vacuum to characterize the significance of environmental effects on fatigue life.

In order to determine all the necessary data for the application of selected fracture mechanics life prediction models without any fitting, creep tests were performed in conventional creep machines, which were modified in such a way that the stress could be kept constant in each

test. Furthermore, fatigue crack growth was studied using single edge notch specimens loaded in 4-point bending.

Microstructural changes were characterized applying TEM on samples which were thinned either using conventional twin-jet electropolishing (IMI 834) or ion milling (X8019 and X8019/12.5_p). Scanning electron microscopy (SEM) was used to determine the relevant damage mechanisms. Microhardness profiles were measured on samples of IMI 834, since this alloy forms an oxygen-enriched brittle subsurface layer (α -case) during high-temperature exposure to air. As shown below, this oxygen embrittlement is enhanced by cyclic plastic deformation and contributes significantly to fatigue crack propagation. Since hardness within this layer is approximately proportional to the square root of the oxygen concentration (Liu & Welsch 1988), microhardness profiles provide a simple means to quantify the depth of this zone.

The main results of the isothermal fatigue tests and the TMF experiments have been published in detail earlier (Pototzky *et al* 1998, 2000; Jung *et al* 1998a, 2000; Hardt *et al* 1999). The description of the fatigue behaviour is confined in this paper to those aspects which are relevant in the context of the fracture mechanics life prediction methods used. Results reported in the literature (Sarrazin-Baudoux *et al* 1996; Lestrin *et al* 1996, Nowack & Kordisch 1998) were employed where model parameters could not be determined from the experiments performed.

3. Selected fracture mechanics concepts and their application

3.1 Cyclic J integral

3.1a *Theoretical background:* In the case of Ni-base superalloys, fatigue crack propagation can be described by means of linear-elastic fracture mechanics even at high temperatures. The ductile and less creep resistant alloys dealt with in this study require a consideration of the effect of non-elastic deformation on crack growth. According to the concept proposed by Dowling (Dowling 1977), the cyclic J integral can be applied for conditions where a solely cycle-dependent behaviour is observed. Following Heitmann *et al* (1984), an approximation for semicircular cracks under plain strain conditions can be used to calculate the effective cyclic J integral as

$$\Delta J_{\text{eff}} = (2.9W_{\text{el,eff}} + 2.5W_p) a = Z_D a. \quad (1)$$

$W_{\text{el,eff}}$ and W_p are the effective elastic and the plastic deformation strain energy densities respectively and a denotes the crack length. Both energy densities can directly be determined from the stress–strain response of cyclic deformation. W_p is represented as the area under the ascending branch of the hysteresis loop in a plot of stress σ vs plastic strain ε_{pl} . Crack closure effects are accounted for in $W_{\text{el,eff}}$ using

$$W_{\text{el,eff}} = (\Delta\sigma_{\text{eff}})^2 / 2E, \quad (2)$$

where E is Young's modulus. The effective stress range $\Delta\sigma_{\text{eff}}$ can be calculated in a first approximation from the stress range $\Delta\sigma$ and the load ratio R using (Heitmann *et al* 1984),

$$\Delta\sigma_{\text{eff}} = 3.72\Delta\sigma(3 - R)^{-1.74}. \quad (3)$$

The crack propagation rate (da/dN) is assumed to follow (4) below so that the number of cycles to failure N_f results from an integration of this equation from the initial crack length a_0 at N_0 (which is 1 according to the concept) to the final crack length a_f .

$$da/dN = C(\Delta J_{\text{eff}})^m = C(Z_D)^m a^m, \quad (4)$$

$$N_f \{ [(a_f)^{1-m} - (a_0)^{1-m}] / [(1-m)C(Z_D)^m] \} + N_0. \quad (5)$$

For the application of this concept it is very advantageous if the crack propagation constants C and m in (4) and (5) can be derived directly from the Paris regime of fatigue crack growth under linear elastic fracture mechanics conditions. Under plane strain conditions ΔJ_{eff} and the effective stress intensity range ΔK_{eff} are related via

$$\Delta J_{\text{eff}} = (\Delta K_{\text{eff}})^2 (1 - \nu^2) / E, \quad (6)$$

where ν is Poisson's ratio.

3.1b Application of cyclic J integral to X8019 and X8019/12.5 $_p$: The results of fatigue life prediction according to (5) depend to a large extent on the value assumed for a_0 . SEM study revealed that in particle-reinforced material the fatigue crack always starts from cracked or debonded large SiC particles located at or close to the surface. Hence, irrespective of temperature an initial crack length of $15\mu\text{m}$ was determined metallographically, which corresponds reasonably well with the diameter of the largest SiC particles. In the SiC-free material, cracks are also formed very early in life starting from the surface in areas which appear brittle. However, metallographic inspection indicated that the initial crack size increases with temperature from a value of $8\mu\text{m}$ at room temperature to $15\mu\text{m}$ at 300°C . In both materials fatigue crack propagation seems to govern cyclic life up to temperatures of 250°C where creep deformation can no longer be neglected.

In the case of reinforced alloy a change in damage mechanism both with increasing temperature under isothermal conditions and with strain-temperature phasing of TMF was observed. In isothermal tests at room temperature as well as in TMF OP tests, crack propagation takes place mainly within the matrix. Cracked SiC particles were only found on the fracture surface, i.e., cracking occurs in the stress field of the propagating crack without strong effect on crack growth rate. In the areas remote from the main crack, debonding of particles occurred (see figure 3a) without cracking. At elevated temperature and under TMF IP conditions, voids are formed at the SiC/matrix interface (see figure 3b) as a bulk phenomenon, and cracking in front of the growing crack seems to lose importance. Thus under these conditions fatigue cracks first extend preferentially within the matrix and later propagate by link-up with the SiC/matrix interface voids.

Since neither creep deformation nor void formation is contained in the ΔJ concept, its application is only justified at low temperatures ($< 250^\circ\text{C}$). The lines in figure 4 represent the result of the calculation according to (5) carried out for room temperature on the basis of a final crack size of $1\mu\text{m}$ and values of C and m from long fatigue crack growth tests (4-point bending). The symbols depict the experimentally determined fatigue lives. Reasonable agreement between calculation and experiment is obtained.

3.1c Application of cyclic J integral to IMI 834: As has been stated above, the ΔJ concept is very sensitive to a_0 while it is rather insensitive to a_f . This fact was used to indirectly determine the initial crack size as a function of temperature for IMI 834 by adapting a_0 in (5) in such a way that it yields the values of N_f of fatigue tests carried out in high vacuum. Since

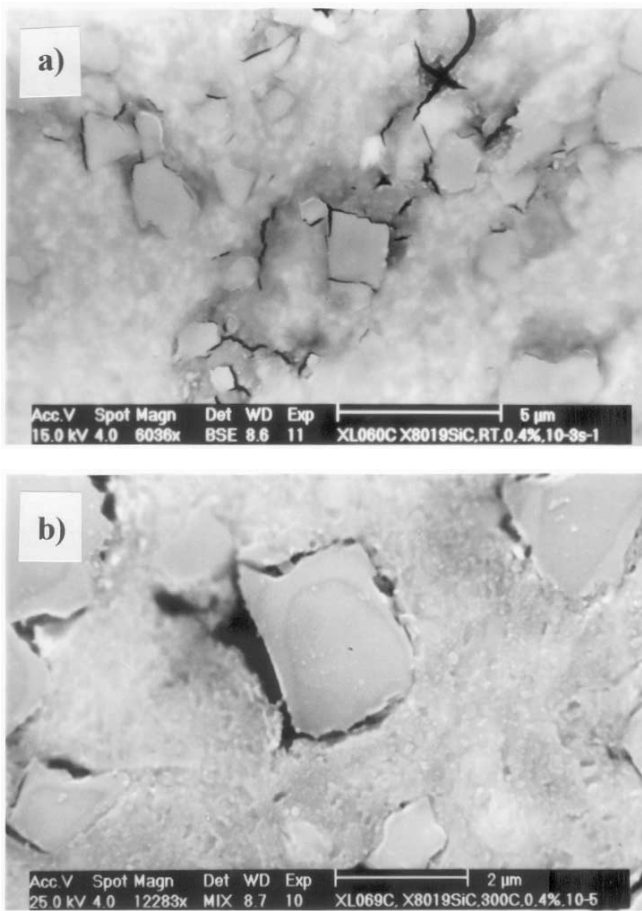


Figure 3. SEM micrographs of longitudinal sections of specimens cyclically loaded at a plastic strain amplitude of 0.4% at (a) room temperature and (b) 300°C (stress axis is vertical).

environmental effects can be excluded in vacuum and creep deformation was found to be negligible under the test conditions applied, this procedure seems to be justified. Moreover, it

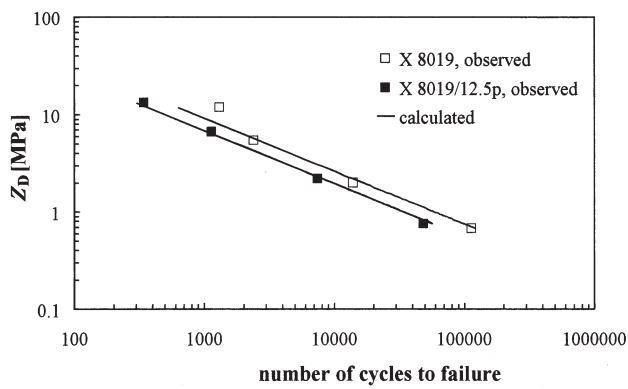


Figure 4. Comparison of experimentally obtained and calculated lives at room temperature for X8019 and X8019/SiC_p as a function of Z_D .

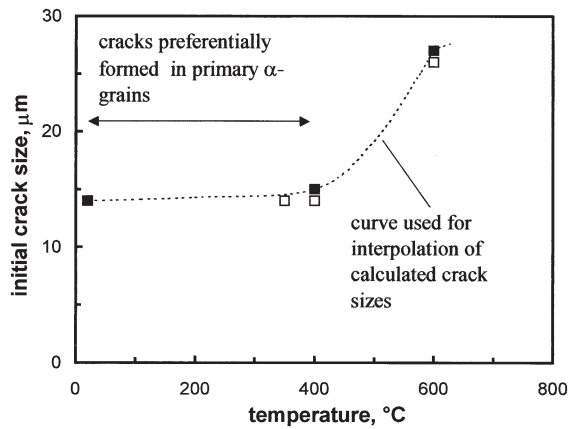


Figure 5. Initial crack size in IMI 834 as a function of temperature in isothermal tests at a plastic strain amplitude of 2×10^{-2} ; ■ calculated from fatigue life obtained in vacuum tests, □ observed by means of metallographic inspection.

provides the basis to estimate the contribution of pure fatigue damage under complex loading conditions as will be shown later. The resulting values of a_0 are plotted versus temperature in figure 5.

In order to check whether the calculated increase of the initial crack size with temperature represents the real behaviour, SEM was employed. Figures 6 and 7 show typical examples for crack initiation sites as observed after cyclic deformation at low and high temperature, respectively. Up to a testing temperature of about 400°C, most cracks are formed within the primary α grains (figure 6). At higher magnification, it becomes apparent that cracks initiate along planar slip bands. Consequently, a_0 should be identical to the primary α grain size (14 μ m). Hence, the values seen in figure 5 in the low temperature plateau is in excellent accordance with the metallographically determined ones.

The increase of a_0 is also reflected in the SEM study. The few fatigue cracks which were found in the primary α grains at $T = 600^\circ\text{C}$ seem to become non-propagating as soon as they reach the grain boundary. The cracks formed in the transformed α grains (the prior β grains) and seem to grow rather unhindered (figure 7). Therefore, the prior β grain size, which is about

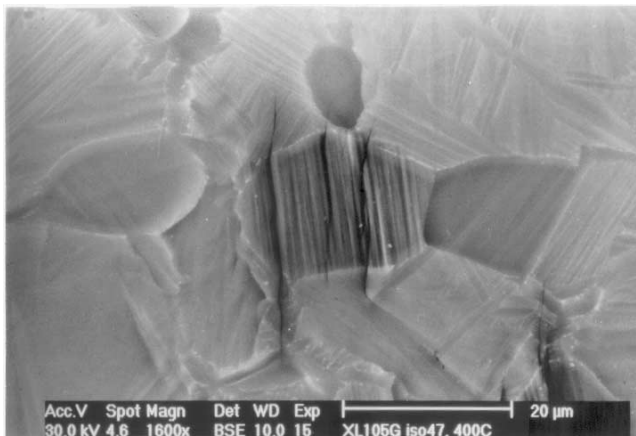


Figure 6. SEM micrographs showing typical crack initiation sites for tests run at $T = 400^\circ\text{C}$ (stress axis is horizontal).

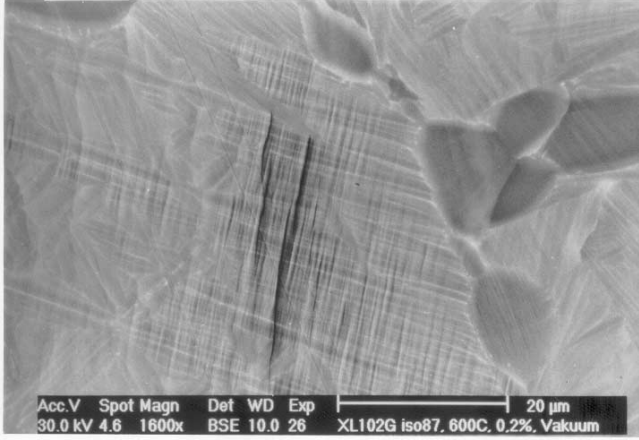


Figure 7. SEM micrograph showing typical crack initiation sites for tests run at $T = 600^\circ\text{C}$ (stress axis is horizontal).

$25\ \mu\text{m}$, provides a reasonable value for a_0 at high temperature in accordance to figure 5. A possible explanation for this change in the crack initiation mechanism is given in Maier *et al* 2000.

3.2 Creep-fatigue damage parameter D_{CF}

Different from the behaviour of IMI 834, creep was found to contribute significantly to cyclic plastic deformation during fatigue testing of X8019 and X8019/12.5_p at temperatures above 250°C . Fractography showed the void formation at the SiC particles in the reinforced material (see figure 3b). However, this creep damage mechanism seems to occur independently of fatigue damage which is still governed by crack growth within the dispersion-strengthened matrix.

Riedel (1987) proposed an extension of the ΔJ approach for exactly this situation that void formation and crack propagation are not coupled. Then the crack growth rate depends on the creep-fatigue damage parameter D_{CF} as

$$da/dN = C(D_{CF})^m a^m. \quad (7)$$

Using some simplifying approximations which are described in Riedel 1987, D_{CF} can be expressed as

$$D_{CF} = 2.9 \left[\Delta\sigma_{\text{eff}}^2 / 2E \right] + 2.4(1 + 3/n)^{1/2} \Delta\sigma \Delta\varepsilon_{\text{pl}} \left[1 + (\Delta\varepsilon_{\text{cr}} / \Delta\varepsilon_{\text{pl}})^{1+n'} \right], \quad (8)$$

where n denotes the Norton exponent which was determined in constant-stress creep experiments, and n' is the fatigue hardening exponent that was calculated from the slope of the cyclic stress-strain curve. The separation of plastic strain range $\Delta\varepsilon_{\text{pl}}$ and creep strain range $\Delta\varepsilon_{\text{cr}}$ for isothermal push-pull loading was carried out with reasonable accuracy by means of fatigue tests that employed instantaneous changes in strain rate (Jung *et al* 1998b). All the other parameters were treated exactly as described above in the context of the application of ΔJ so that no fitting was required.

Figure 8 compares the experimentally determined number of cycles to failure with the prediction results for both the reinforced and the SiC-free material at 300°C and a plastic

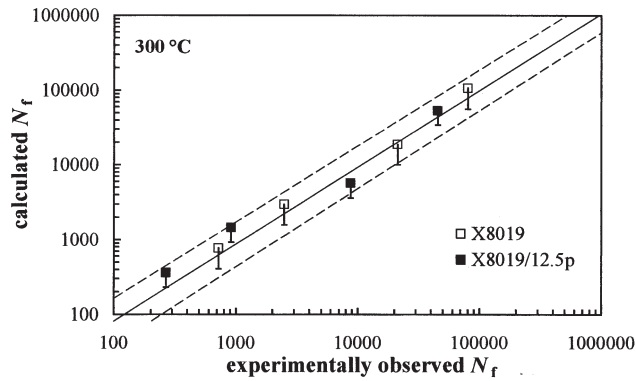


Figure 8. Comparison of experimentally obtained and calculated lives at 300°C for X8019 and X8019/SiC_p at a plastic strain rate of 10^{-3} s^{-1} .

strain rate of 10^{-3} s^{-1} . The error bars correspond to the variation of the initial crack length as observed fractographically. It must be emphasized that a reasonable agreement can only be expected if the loading conditions applied fulfill the requirements for an application of D_{CF} . In particular, if the temperature is too high or the plastic strain rate too low, a strong interaction of creep cavity formation and crack growth may become significant, or lifetime may even be exclusively determined by creep damage evolution.

The transition to the region where creep dominates and corresponding parameters such as C^* apply can be defined by comparing the stress amplitudes of fatigue tests with the stresses from creep tests on the basis of the plastic strain rate used for cyclic loading and measured as steady state creep rate under monotonic conditions, respectively. Figure 9 represents fatigue data as open symbols, while creep data are plotted as full symbols. The change in slope from the fatigue line to the creep line indicates that below a critical plastic strain rate, which increases with temperature, the behaviour is dominated by creep.

3.3 Considering environmental effects on isothermal fatigue and TMF life of IMI 834

3.3a *Basic concept:* Environmental effects are known to play an important role in high-temperature fatigue of titanium alloys. Since the dominant mechanism of the interaction of IMI 834 with laboratory air changes with temperature and this change takes place in each

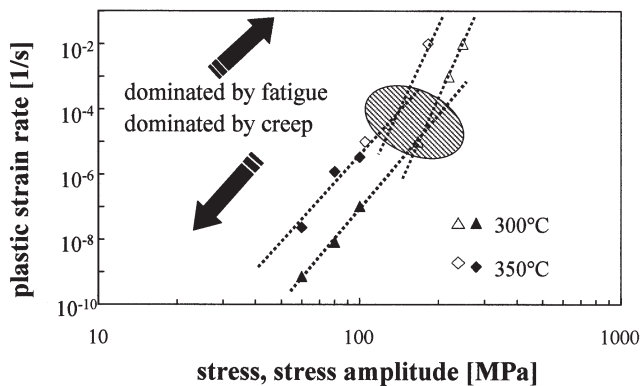


Figure 9. Strain rate as a function of stress or stress amplitude for X8019/12.5_p; full symbols represent creep tests, open symbols show results from fatigue tests.

TMF cycle, it is necessary in a suitable life prediction model to treat the environmental effects separately instead of considering them implicitly in the fatigue crack growth law as done so far for the aluminum alloys studied. On the other hand, systematic investigations applying various types of load cycles including those incorporating dwell periods (Nowack & Kordisch 1998; Hardt *et al* 1999) documented that creep damage is negligible in the temperature range relevant to technical use. Even in creep tests large plastic strains must be accumulated to cause void formation. Hence, for modelling it is assumed that the overall crack growth rate contains two contributions which account for pure fatigue and environmental effects. For the sake of simplicity a linear superposition law was applied:

$$\frac{da}{dN} = \left. \frac{da}{dN} \right|_{\text{fat}} + \left. \frac{da}{dN} \right|_{\text{env}}. \quad (9)$$

The term in (9) that corresponds to pure fatigue was expressed by means of the ΔJ concept (equation (4)) as described above. Since the crack propagation behaviour of titanium alloys in high vacuum is almost independent of temperature, data observed at room temperature on long fatigue cracks were used (Nowack & Kordisch 1998).

3.3b Environmental effect at high temperature: Microhardness profiles obtained on cyclically deformed samples documented that oxygen uptake is aided by plastic deformation. At temperatures above 600°C fatigue crack propagation is strongly affected by the existence of an oxygen-embrittled subsurface zone. Following the suggestion of Reuchet & Rémy (Reuchet & Rémy 1983), the thickness of this zone e_m can be described by

$$e_m = \alpha_m \sqrt{t} = \alpha_m^0(T) (1 + K_m(\Delta\varepsilon_{\text{pl}}/2)) \sqrt{t}, \quad (10)$$

where K_m is a constant and α_m^0 denotes the oxidation constant without cyclic loading, i.e., at zero plastic strain amplitude $\Delta\varepsilon_{\text{pl}}/2$. As the number of cycles N increases, the crack propagates faster, and the environmental contribution to fatigue crack velocity decreases. Different to Reuchet and Rémy, who assumed that $da/dN|_{\text{env}}$ is independent of N , the total crack advance due to the environment was assessed to be equal to the a-case layer thickness at the smooth surface determined metallographically, i.e.

$$da/dN|_{\text{env}} = de_m(t)/dN = d(\alpha_m \sqrt{\tau N})/dN = \alpha_m/2 (\tau/N)^{1/2}, \quad (11)$$

where τ is the cycle time. Inserting (11) and (4) into (9) results in an equation that cannot be integrated in closed form. Therefore, the number of cycles to failure was calculated using the Euler-Cauchy iteration method.

3.3c Environmental effect at intermediate temperature: Oxygen uptake in high-temperature titanium alloys becomes negligible for temperatures below about 500°C. As shown by comparative studies on the fatigue crack propagation in nitrogen and humidified air (Sarrazin-Baudoux *et al* 1996; Lesterin *et al* 1996) the main environmental degradation can be attributed to hydrogen which results from the reaction of water vapour with the freshly exposed crack tip. Unfortunately, this type of environmental effect on fatigue crack growth cannot be proved directly by metallographic studies. Hence published data on long fatigue crack growth was used to quantitatively describe the detrimental environmental effect in the intermediate temperature range. The expression

$$da/dN|_{\text{env}} = (H_1 H_2) da/dN|_{\text{fat}} \quad (12)$$

was applied where H_1 was derived from the increase in fatigue crack growth rate observed in humidified argon as compared to high vacuum (Lesterin *et al* 1996). The parameter H_2 takes the effect of frequency into account and was deduced from test results observed at 0.5 and 35 Hz (Sarrazin-Baudoux *et al* 1996). Since the effect of temperature and stress intensity factor range on H_1 and H_2 has been shown to be very small, constant values were assumed.

3.3d *Application to isothermal fatigue and TMF:* So far the concept presented is applicable to isothermal conditions only. In this case the environmental degradation is mostly dominated by one damage mechanism which is determined by temperature. In order to describe the behaviour in the temperature range of a TMF cycle, it is assumed that both environmental effects are decoupled and therefore oxygen and hydrogen contribution are combined by means of a linear superposition.

$$\left. \frac{da}{dN} \right|_{\text{env}} = \left. \frac{da}{dN} \right|_{\text{Oxygen}} + \left. \frac{da}{dN} \right|_{\text{Hydrogen}} \quad (13)$$

Figures 10a–c represent the maximum stress values observed in fatigue tests at various temperatures in vacuum and ambient air as a function of the number of cycles to failure. Fatigue life in vacuum is reasonably well predicted on the basis of the assumption of pure fatigue, (5), as seen by the straight line in figures 10a–c. The curve labelled “dry air” in figure 10a represent the calculation results for dry air ((4), (9) and (11)). The curved dashed line in figure 10b shows the result calculated for humid argon environment ((4), (9) and (12)). The linear combination of both environmental damage contributions according to (13) yields very satisfactory results in the whole temperature range (see curve C in figure 10c).

Previous work (Maier & Christ 1997) has shown that TMF hysteresis loops can be modelled for many materials based only on isothermal data. Hence, TMF fatigue life in an *inert* environment can be predicted in a straightforward manner from isothermal data using the cyclic J integral concept introduced above. However, the question of the initial crack size needs to be addressed. SEM investigation shows that the change in a_0 with temperature observed under isothermal conditions (see figure 5) does not occur in TMF. Crack nucleation is always observed in the lamellar transformed β matrix. In other words, initial crack size is assumed to be governed by the maximum temperature of the TMF cycle.

The consideration of environmental effects on fatigue life in TMF is more complicated and demands additional assumptions. Hydrogen embrittlement is assumed to be negligible in the case of IP TMF as stresses are mostly compressive in the low-temperature part of the cycle. Consequently, oxidation is the only environmental effect considered for IP TMF. By contrast, both environmental degradation mechanisms are accounted for to predict N_f of OP TMF tests. Oxygen uptake is assumed to be unaffected by the sign of the stress and therefore should be rather independent of plastic strain-temperature phasing. Since high tensile stresses coincide with low temperature in OP TMF, hydrogen embrittlement must be expected due to the reaction of the alloy with water vapour.

Figure 11 compares the experimentally observed TMF lives of IP and OP tests at two values of the plastic strain amplitude with the results of the prediction calculation. As can be seen, all data points lie within $a \pm 2$ scatter band.

3.4 TMF life prediction for X8019 and X8019/12.5_p

In contrast to most of the isothermal tests carried out on both aluminum alloys, TMF tests were performed applying a low plastic strain rate of 10^{-5} s^{-1} . This fact and the periodically

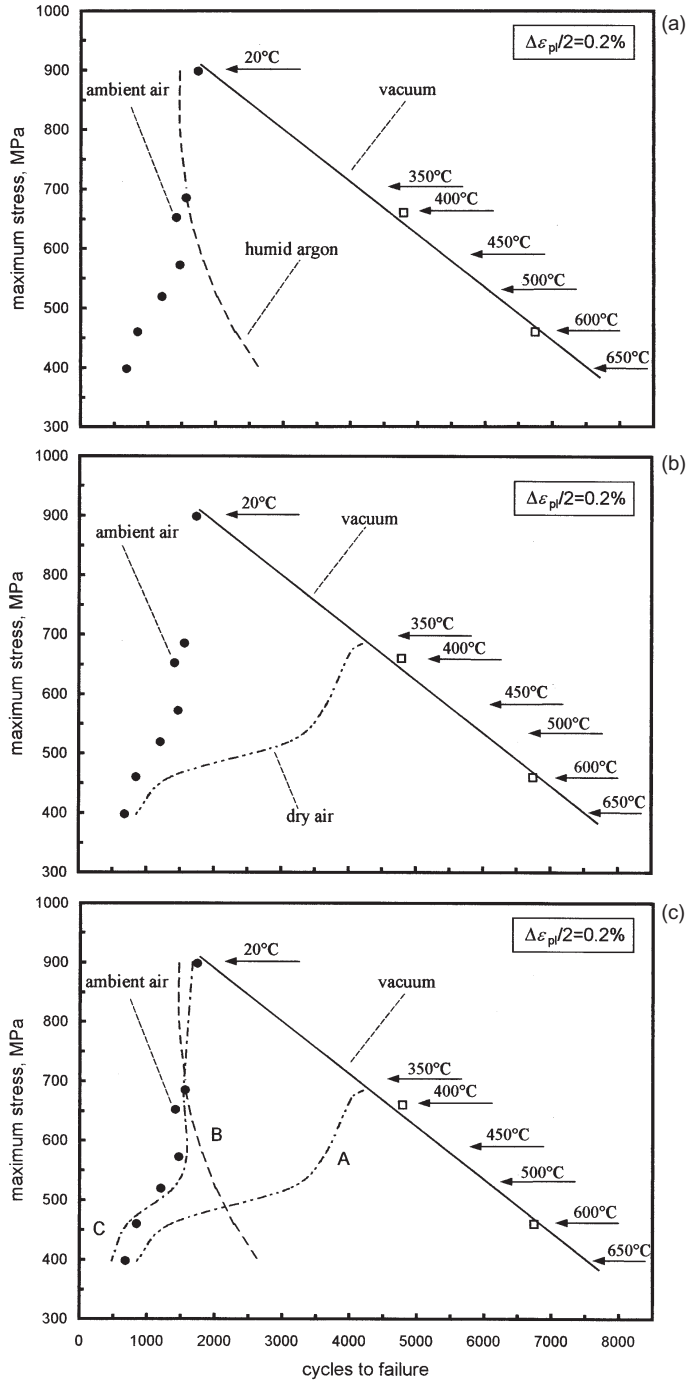


Figure 10. Comparison of the values of N_f observed in vacuum (\square) and air (\bullet) with prediction results obtained on the basis that (a) only pure fatigue and oxidation damage are relevant, (b) only pure fatigue and environmental degradation resulting from the reaction of the alloy with water vapour occur, and (c) both environmental effects and fatigue damage are superimposed.

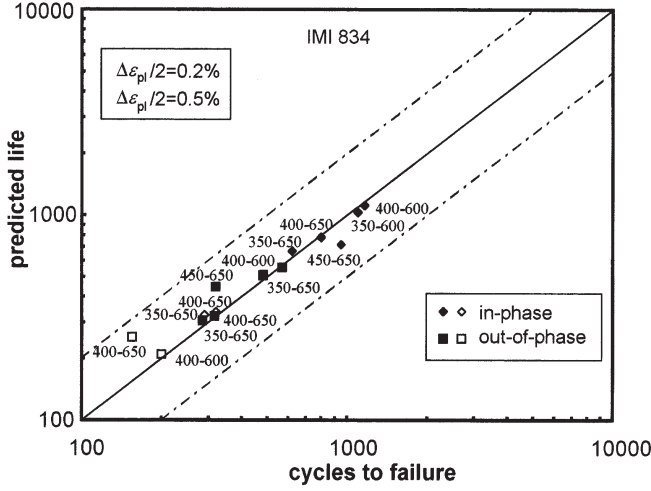


Figure 11. Comparison of experimentally obtained and calculated lives for IMI 834 under TMF conditions at plastic strain amplitudes of 0.2% (closed symbols) and 0.5 (open symbols). Temperature range of test is given next to symbol.

changing temperature in TMF demands again a separate treatment of the oxidation damage contribution. Moreover, no solution is known yet for the D_{CF} parameter under non-isothermal conditions. Hence, a combined consideration of creep and fatigue contribution to damage evolution by means of D_{CF} is not possible for TMF. Therefore, the following basic equation was used assuming that there is no coupling between the single damage mechanisms.

$$\frac{da}{dN} = \left. \frac{da}{dN} \right|_{\text{fat}} + \left. \frac{da}{dN} \right|_{\text{Creep}} + \left. \frac{da}{dN} \right|_{\text{Oxygen}}. \quad (14)$$

Fatigue crack growth rate under pure fatigue conditions can be calculated directly applying (4). As crack propagation was found to occur within the matrix during most part of fatigue life and time-dependent effects should not be contained in the fatigue term of (14), crack growth data obtained for the unreinforced material at room temperature and high frequency was used. The actual value of ΔJ_{eff} can either be taken from a measured TMF hysteresis loop or calculated from isothermal data taking advantage of the very stable microstructure (Maier & Christ 1997).

Miller *et al* (1993) proposed a method to assess the creep damage from creep rates observed in monotonic creep tests and $\left. \frac{da}{dN} \right|_{\text{Creep}}$ was calculated in this way. However it turned out that the creep damage resulting from TMF is nearly negligible. This is simply a consequence of the strong temperature dependence of the creep rate; creep deformation takes place only close to the maximum temperature of each TMF cycle.

Oxidation damage was treated analogously to the model of Miller *et al* 1993, according to

$$\left. \frac{da}{dN} \right|_{\text{Oxygen}} = C_{O_x} (\Delta J_{\text{eff}})^{m_{O_x}} \tau^{\psi} = C_{O_x}^* \exp(-Q_{O_x}/RT_{\text{eff}}) (\Delta J_{\text{eff}})^{m_{O_x}} \tau^{\psi}, \quad (15)$$

where m_{O_x} and ψ are material constants and τ is the cycle time. The coefficient C_{O_x} accounts for the temperature dependence of oxidation and obeys an Arrhenius-type equation. In the original model, the apparent activation energy Q_{O_x} is a function of the stress at the minimum temperature of the TMF cycle in order to take mean stress effects on cyclic life into account.

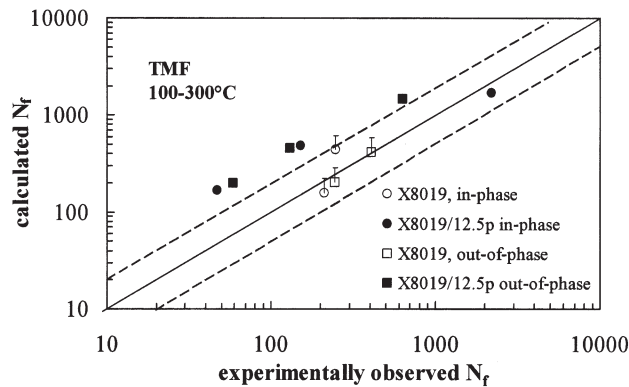


Figure 12. Comparison of experimentally obtained and calculated TMF lives of X8019 and X8019/12.5_p at a plastic strain rate of 10^{-5} s^{-1} .

As N_f of the materials studied was found to be not strongly affected by phasing (OP and IP), this extension was ignored. The oxide formation on aluminum alloys occurs quite rapid as soon as the material is exposed to air and leads to a thin layer of approximately constant thickness. The oxidation rate and hence the relevant oxide thickness in TMF is governed by the maximum temperature T_{\max} in the cycle. Therefore, the effective temperature T_{eff} in (15) was replaced by T_{\max} . All the other oxidation parameters of (15) were obtained by non-linear least squares regression to *isothermal* fatigue life data from tests performed on *unreinforced* material

Figure 12 shows a comparison of the calculated values for TMF life and the experimentally observed ones. As discussed in detail by Jung *et al* (2000) a non-conservative prediction results for the particle-reinforced material that can be attributed to the fact that coupling of the damage mechanisms occurs which is not taken into account in the model.

4. Concluding remarks

In principle, the concepts described throughout this paper and the prediction results obtained by using these concepts show that fracture mechanics methods are a suitable means to describe fatigue life both for isothermal and thermomechanical conditions. However, the description given here indicates that the concepts must be selected carefully in such a way that they relate closely to relevant damage mechanisms and microstructural changes. Hence, no fracture mechanics damage parameter is *a priori* qualified. Rather extensive testing in combination with detailed microstructural and fractographic studies have to be carried out, before an appropriate concept can be selected. This line of action is illustrated for the alloy X8019/12.5_p by means of figures 13 and 14. In figure 13, a map is presented which shows the regimes of plastic strain amplitude (ordinate) and temperature or plastic strain rate (abscissa) where damage can be attributed to fatigue, creep or oxidation and combinations of these damage types. On the basis of such a map, which results from metallographic inspection of correspondingly tested samples, suitable damage parameter can be chosen and allocated to the respective loading parameter regime (see figure 14). In the case of TMF, adaptation of these concepts to non-isothermal conditions requires several considerations that include the adaptation and mechanistic aspects.

A fundamental disadvantage that arises from the strong connection of the relevant damage processes with the suitable fracture mechanics parameter is the very restricted transferability

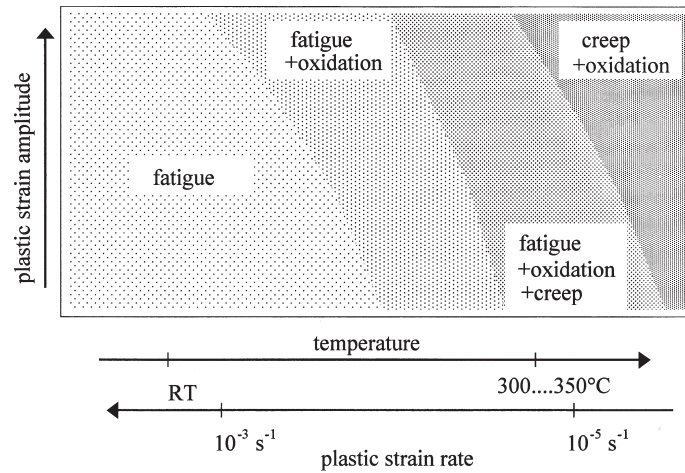


Figure 13. Schematic map representing the regimes of the relevant main origins for damage as a function of testing parameters for X8019/12.5p.

of corresponding models to new loading conditions. This might be an important reason why empirical life prediction methods are still preferred in practical applications. Despite the lack of physical reasoning, empirical approaches provide similar predictive accuracy (compare Maier *et al* 2002) and are simpler to apply. However, the acceptable range of applicability and the transferability are better defined for fracture mechanics methods, if a sound knowledge on the active damage mechanisms exists. Furthermore, in research the application of fracture mechanics can help to identify those mechanisms which control damage evolution and to quantify these processes.

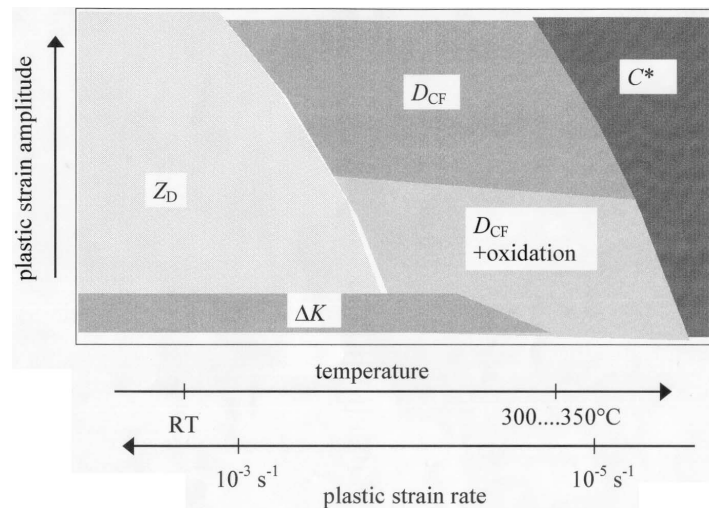


Figure 14. Schematic map representing the regimes of the respective life prediction concepts deduced from figure 13 for X8019/12.5p.

One major limitation of *simple* fracture mechanics concepts has been illustrated above in the form of the poor accuracy of the calculated TMF life of X8019/12·5_p (see figure 12). Since a linear combination of damage contribution has been used in the model applied, the unsatisfactory prediction result is not surprising, but simply a consequence of coupling of damage mechanisms as confirmed by metallographic observations. There are some models proposed in the literature which try to take these interactions into account. At present however, it appears that the understanding of the physical nature of these coupling effects and even more a mathematical description of the relevant processes are much too incomplete to provide an appropriate basis for a model development.

The authors are grateful to Deutsche Forschungsgemeinschaft for supporting this study financially.

References

- Angers L, Fine M E, Weertman J R 1987 Effect of plastic deformation on the coarsening of dispersoids in a rapidly solidified Al-Fe-Ce alloy. *Metall. Trans.* A18: 555–562
- ASME 1994 ASME Boiler and Pressure Vessel Code: Section 3, Rules for construction of nuclear Power Plant Components, New York
- Bernstein H L, Grant T S, McClung R C, Allen J M 1993 Prediction of thermal-mechanical fatigue life for gas turbine blades in electric power generation. *Thermomechanical fatigue behaviour of materials* (ed.) H Sehitoglu, ASTM STP 1186 (Philadelphia, PA: ASTM) pp 212–238
- Chaboche J L, Lesne P M 1988 A non-linear continuous fatigue damage model. *Fatigue Fracture Eng. Mater. Struct.* 11: 1–17
- Christ H -J, Mughrabi H, Kraft S, Petry F, Zauter R, Eckert K 1996 The use of plastic strain control in thermomechanical fatigue testing. *Fatigue under thermal and mechanical loading – Mechanisms, mechanics and modelling* (eds) J Bressers, L Rémy (Dordrecht: Kluwer Academic) pp 1–14
- Dai J, Marchand N J, Hongoh M 1996 Thermal mechanical fatigue crack growth in titanium alloys: Experiments and modelling. *Thermomechanical fatigue behaviour of materials: second volume* (eds) M J Verrilli, M G Castelli, ASTM STP 1263 (West Conshohocken, PA: ASTM) pp 187–209
- Danzer R 1988 *Lebensdauerprognose hochfester metallischer Werkstoffe im Bereich hoher Temperaturen* (Berlin–Stuttgart: Gebrüder Bornträger)
- Dowling N E 1977 Crack growth during low-cycle fatigue of smooth axial specimens. *Cyclic stress-strain and plastic deformation* (ed.) L F Impellizzeri, ASTM STP 637 (Philadelphia, PA: ASTM) pp 97–121
- Ellison E G, Al-Zamily A 1994 Fracture and life prediction under thermal-mechanical strain cycling. *Fatigue Fracture Eng. Mater. Struct.* 17: 53–57
- Halford G R, Lerch B A, Arya V K 2000 Thermal strain fatigue modeling of a matrix alloy for a metal matrix composite. *Thermomechanical fatigue behaviour of materials: third volume* (eds) H Sehitoglu, H J Maier, ASTM STP 1371 (West Conshohocken, PA: ASTM) pp 186–203
- Halford G R, Manson S S 1976 Life prediction of thermal-mechanical fatigue using strain range partitioning. *Thermal fatigue of materials and components* (eds) D A Spera, D F Mowbray, ASTM STP 612 (Philadelphia, PA: ASTM) pp 239–254
- Hardt S, Maier H J, Christ H -J 1999 High-temperature fatigue damage mechanisms in near-alpha titanium alloy IMI 834. *Int. J. Fatigue* 21: 779–789
- Heitmann H H, Vehoff H, Neumann P 1984 Life prediction for random load fatigue based on the growth behaviour of microcracks. *Advance in Fracture Research (ICF6)* (eds) S R Valluri, D M R Tuplin, P R Rao, J F Knott, R Dublex (New Delhi: Pergamon) pp 3566–3606

- Jordan E H, Meyers G J 1986 Fracture mechanics applied to nonisothermal fatigue crack growth. *Eng. Fracture Mech.* 23: 345–358
- Jung A 2000 *Einfluss einer Partikelverstärkung auf das Hochtemperaturermüdungsverhalten einer dispersionsgehärteten Aluminiumlegierung*. Doctorate thesis, Universität Siegen, Germany
- Jung A, Maier H J, Christ H-J 1998a High-temperature fatigue behaviour and microstructure of a dispersoid-strengthened and SiC-reinforced aluminium alloy. *Microstructure and mechanical properties of metallic high-temperature materials* (eds) H Mughrabi, G Gottstein, H Mecking, H Riedel, J Tobolski (Weinheim, Germany: Wiley-VCH-Verlag) pp 34–49
- Jung A, Maier H J, Christ H-J 1998b Low-cycle fatigue behaviour and lifetime prediction of a SiC-particulate reinforced aluminium alloy at elevated temperatures. *Proc. 12th Conf. on Fracture (ECF12)* (eds) M W Brown, E R de los Rios, K J Miller, pp 303–308
- Jung A, Maier H J, Christ H-J 2000 Effect of SiC-reinforcement on thermomechanical fatigue of a dispersion-strengthened high-temperature aluminum alloy. *Thermomechanical fatigue behaviour of materials: third volume* (eds) H Sehitoglu, H J Maier, ASTM STP 1371 (West Conshohocken, PA: ASTM) pp 167–185
- Kadioglu Y, Sehitoglu H 1996 Thermomechanical and isothermal fatigue behaviour of bar and coated superalloys. *J. Eng. Mater. Technol.* 118: 94–102
- Lesterin S, Sarrazin-Baudoux C, Petit J 1996 Temperature-environment interactions on fatigue behaviour in Ti6246 alloy. *Titanium '95: Science and Technology* (eds) P A Blenkinsop, W J Evans, H M Flower (London: Institute of Materials) pp 1211–1218
- Liu Z, Welsch G 1988 Effects of oxygen and heat treatment on the mechanical properties of alpha and beta titanium alloys. *Metall. Trans.* A19: 527–542
- Maier H J, Christ H-J 1997 Modeling of cyclic stress-strain behaviour and damage mechanisms under thermomechanical fatigue conditions. *Int. J. Fatigue* 19 (Suppl): 267–274
- Maier H J, Teteruk R G, Christ H-J 2000 Modeling thermomechanical fatigue life of high-temperature titanium alloy IMI 834. *Metall. Mater. Trans.* A31: 431–444
- Maier H J, Teteruk R, Christ H-J 2002 Modelling thermomechanical fatigue life. *Materials at high temperatures* (in print)
- Miller M P, McDowell D L, Oehmke R L T, Antolovich S D 1993 A life prediction model for thermomechanical fatigue based on microcrack propagation. *Thermomechanical fatigue behaviour of materials* (ed.) H Sehitoglu, ASTM STP 1186 (Philadelphia, PA: ASTM) pp 35–49
- Neal D F 1985 Optimization of creep and fatigue resistance in high temperature titanium alloys IMI 829 and IMI 834. *Titanium science and technology* (eds) G Lütjering, U Zwicker, W Bunk (Oberursel: Deutsche Gesellschaft für Metallkunde) pp 2419–2424
- Neu R W, Sehitoglu H 1989 Thermo-mechanical fatigue, oxidation and creep: Part II - Life prediction. *Metall. Trans.* A20: 1769–1767
- Nowack H, Kordisch T 1998 Kriech-Ermüdungsverhalten der Titanlegierung IMI 834 bei 600°C. *Materialwissensch. Werkstofftech.* 29: 215–228
- Okazaki M, Koizumi T 1983 Crack propagation during low cycle thermal-mechanical and isothermal fatigue at elevated temperatures. *Metall. Trans.* A14: 1641–1648
- Pototzky P 1999 *Thermomechanischer Ermüdungsverhalten der Hochtemperaturtitanlegierung IMI 834*. Doctorate thesis, Universität Siegen, Germany
- Pototzky P, Maier H J, Christ H-J 1998 Thermomechanical fatigue behaviour of the high-temperature titanium alloy IMI 834. *Metall. Mater. Trans.* A29: 2995–3004
- Pototzky P, Maier H J, Christ H-J 2000 Behaviour of the high-temperature titanium alloy imi 834 under thermomechanical and isothermal fatigue conditions. *Thermomechanical fatigue behaviour of materials: third volume* (eds) H Sehitoglu, H J Maier, ASTM STP 1371 (West Conshohocken, PA: ASTM) pp 18–35
- Rémy L, Bernard H, Malpertu J L, Rezai-Aria F 1993 Fatigue life prediction under thermal-mechanical loading in a nickel-base superalloy. *Thermomechanical fatigue behaviour of materials* (eds) H Sehitoglu, ASTM STP 1186 (Philadelphia, PA: ASTM) pp 3–16

- Reuchet J, Rémy L 1983 Fatigue oxidation interaction in a superalloy - Application to life prediction in high temperature low cycle fatigue. *Metall. Trans. A14*: 141–149
- Riedel H 1987 *Fracture at high temperatures* (eds) B Ilschner, N J Grant (Berlin: Springer)
- Sarrazin-Baudoux C, Lesterin S, Petit J 1996 Atmospheric influence on fatigue crack propagation in TiAl6V alloy up to 300°C. *Titanium '95: Science and technology* (eds) P A Blenkinsop, W J Evans, H M Flower (London: Institute of Materials) pp 1895–1902
- Skelton R P 1983 Crack initiation and growth in simple metal components during thermal cycling. *Fatigue at high temperature* (eds) R P Skelton (London: Applied Science Publishers) pp 1–63
- Teteruk R 2001 *Modellierung der Lebensdauer bei thermomechanischer Ermüdungsbeanspruchung unter Berücksichtigung der relevanten Schädigungsmechanismen*. Doctorate thesis, Universität Siegen, Germany
- Woodford D A, Mowbray D F 1974 Effect of materials characteristics and test variables on thermal fatigue of cast superalloys. *Mater. Sci. Eng.* 16: 5–43
- Zamrik S Y, Renauld M L 2000 Thermo-mechanical out-of-phase fatigue life of overlay coated IN-738LC gas turbine materials. *Thermomechanical fatigue behaviour of materials: third volume* (eds) H Sehitoglu, H J Maier (West Conshohocken, PA: ASTM) pp 119–137